

# Closing the gap: Exact maximum likelihood training of generative autoencoders using invertible layers

**Gianluigi Silvestri\***

OnePlanet Research Center  
imec-the Netherlands  
gianluigi.silvestri@imec.nl

**Daan Roos\***

Radboud University  
daan.roos@ru.nl

**Luca Ambrogioni**

Donders Institute for Brain, Cognition and Behaviour  
Radboud University  
l.ambrogioni@donders.ru.nl

## Abstract

In this work, we provide an exact likelihood alternative to the variational training of generative autoencoders. We show that VAE-style autoencoders can be constructed using invertible layers, which offer a tractable exact likelihood without the need for any regularization terms. This is achieved while leaving complete freedom in the choice of encoder, decoder and prior architectures, making our approach a drop-in replacement for the training of existing VAEs and VAE-style models. We refer to the resulting models as Autoencoders within Flows (AEF), since the encoder, decoder and prior are defined as individual layers of an overall invertible architecture. We show that the approach results in strikingly higher performance than architecturally equivalent VAEs in term of log-likelihood, sample quality and denoising performance. In a broad sense, the main ambition of this work is to close the gap between the normalizing flow and autoencoder literature under the common framework of invertibility and exact maximum likelihood.

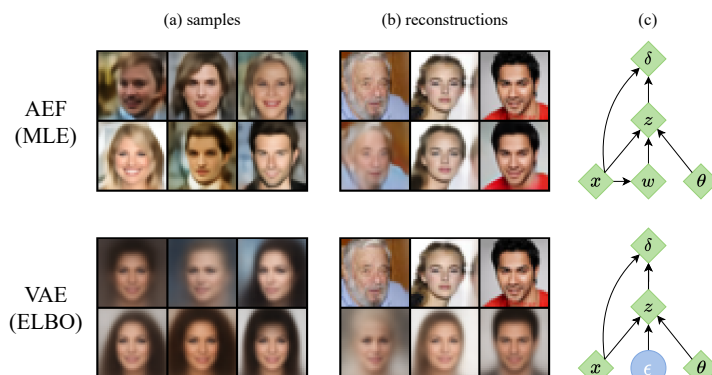


Figure 1: a, b) Comparison of generated and reconstructed CelebA-HQ  $32 \times 32$  images of variational and MLE autoencoders with identical architectures. c) Diagram showing the difference between VAEs and AEF models. The variable  $\delta$  denotes the deviations between the data  $x$  and the prediction based on the latent variable  $z$ .

\*Equal contribution.

# 1 Introduction

Variational autoencoders (VAEs) [41, 60] have maintained an enduring popularity in the machine learning community in spite of the impressive performance of other generative models [25, 36, 72, 70, 65, 18, 59, 19, 39, 66, 51]. One key feature of VAEs is their ability to project complex data into a semantically meaningful set of latent variables. This feature is considered particularly useful in fields such as model-based reinforcement learning, where temporally linked VAE architectures form the backbone of most state-of-the-art world-models [29, 28, 30, 26, 78, 31]. Another attractive feature of VAEs is that they leave ample architectural freedom when compared with other likelihood-based generative models, with their signature encoder-decoder architectures being popular in many areas of ML beside generative modeling [63, 73, 55, 57, 56]. However, VAE training is complicated by the lack of a closed-form expression for the log-likelihood, with the variational gap between the surrogate loss (i.e. the ELBO) and the true log-likelihood being responsible for unstable training and, at least in non-hierarchical models, sub-optimal encoding and sample quality [33, 77, 1, 14, 49]. Consequently, a large fraction of VAE research is devoted to tightening the gap between the ELBO and the true likelihood of the model. Gap reduction can be achieved both by devising alternative lower bounds [7, 2] or more flexible parameterized posterior distributions [59, 40]. Normalizing flows (NF) are deep generative models comprised of tractably invertible layers, whose log-likelihood can be computed in closed-form using the change of variable formula [42, 52]. However, this constraint appears to be at odds with autoencoder architectures, which map all relevant information in a latent space of different (often smaller) dimensionality. This is potentially problematic since naturalistic data such as images and speech waveforms are thought to live, at least approximately, in a lower dimensional manifold of the ambient space [3, 21, 54]. It is therefore common to use hybrid VAE-flow models that deploy NFs for modeling the VAE prior and/or the variational posterior [59, 40]. However, training these models is often a delicate business as changes in the encoder and the prior cause a misalignment from the posterior, increasing the gap and causing a shifting-target dynamics that introduces instabilities and decreases performance. For this reason, the complex autoregressive or flow priors common in modern applications are often trained ex-post after VAE training [71, 58].

In this paper we introduce a new approach for training VAE-style architectures by exact maximum-likelihood. The key insight is that we can formulate an autoencoder within a conventional invertible architecture by using invertible affine layers and by keeping track of the deviations between data and predictions. Importantly, this can be done while leaving complete freedom in the design of the encoder, decoder and prior, which makes our approach a drop-in replacement for the training of existing VAE and VAE-style models. We denote these new generative autoencoders as *autoencoders within flows* (AEF), since the autoencoder architecture is constructed inside a NF architecture.

## 2 Preliminaries

In this section, we will outline the standard theory behind probabilistic generative models. Consider a dataset comprised of data-points  $x \in \mathbb{R}^N$ . We refer to  $\mathbb{R}^N$  as the ambient space. The dataset is assumed to be sampled from a  $D$ -dimensional curved manifold  $\mathcal{M}$  embedded in the ambient space:  $D \subset \{\phi(y) \mid y \in \mathcal{M}\}$  with  $\phi : \mathcal{M} \rightarrow \mathbb{R}^N$  being a differentiable mapping. We refer to  $\mathcal{M}$  as the signal space. A probability measure can be defined on the ambient space by defining a probability density  $p_0(y)$  on  $\mathcal{M}$  and "pushing it through" the mapping  $\phi$ . However, this will not give rise to a proper probability density when  $D < M$  since the signal will span only a subset of possible combinations of ambient values. This pathological behavior can be counteracted by introducing a centered noise density  $p(x \mid y)$  that accounts for data that does not lay on the embedded manifold. **Variational autoencoders:** VAEs are deep generative models in which the density of each data-point depends on  $D$ -dimensional stochastic latent variable  $z \in \mathbb{R}^D$ , which parameterizes the signal space. The emission model is often assumed to be a diagonal Gaussian with parameters determined by deep architectures:  $p(x \mid z_j; \theta) = \mathcal{N}(x_j; f_m(z; \theta), f_\sigma(z; \theta))$ , where  $\theta$  denotes the model parameters. In this formula, the parameterized functions  $f_m(z; \theta)$  and  $f_\sigma(z; \theta)$  are the outputs of a decoder architecture. This corresponds to the parameterized embedded signal manifold  $\{f_m(z; \theta) \mid z \in \mathbb{R}^D\}$ . The emission model is paired with a prior  $p_0(z; \theta)$  over the latents, which is commonly chosen to be a simple standard normal but in modern applications is often itself a parameterized structured model. We can then express the log-likelihood of the data by marginalizing out the latent variables. However, using the marginal log-likelihood as loss function is not practical since the integral is generally intractable. Nevertheless, it is possible to derive a lower bound that can be used as surrogate loss.

This can be done by defining a parameterized approximate posterior model. In the simplest case, this is another diagonal Gaussian distribution:  $q(z | x; \psi) = \mathcal{N}(z; g_m(x; \theta), g_\sigma(x; \theta))$ , where  $g_m(x; \theta)$  and  $g_\sigma(x; \theta)$  are two channels of a decoder architecture. Using this distribution, we can define the evidence lower bound (ELBO):  $\log p(x; \theta) \geq \text{ELBO}(\theta, \psi) = \mathbb{E}_q \left[ \log \frac{p(x|z; \theta) p_0(z; \theta)}{q(z|x; \psi)} \right]$ . This bound becomes tight if  $q(z | x; \psi)$  matches the true posterior. Stochastic estimates of the gradient of the ELBO can be computed by expressing samples from  $q(z | x; \psi)$  as a differentiable deterministic function of standard normal samples:

$$z(x, \epsilon; \psi) = g_m(x; \psi) + g_\sigma(x; \psi) \odot \epsilon, \quad (1)$$

where  $\epsilon$  is a standard normal stochastic input. This is known as reparameterization trick, path derivative estimator or stochastic backpropagation in the variational inference literature [41, 60]. For our purposes, it is important to know that Eq. 1 is an affine invertible layer, like those used in RealNVPs and related NFs [19, 53]. In the simplified case of fixed standard Gaussian prior and unit likelihood variance, this reparameterization of the ELBO leads to the following surrogate objective function for one data-point  $x$ :

$$\mathcal{L}_{\text{VAE}}(\theta, \psi) = \frac{1}{2} \mathbb{E}_\epsilon \left[ \underbrace{\|x - f_m(z(x, \epsilon; \psi); \theta)\|_2^2}_{\text{Reconstruction error}} + \underbrace{\|z(x, \epsilon; \psi)\|_2^2}_{\text{Latent shrinkage}} \right] - \underbrace{\mathcal{H}[q]}_{\text{Entropy regularization}}. \quad (2)$$

The first two terms are a stochastic version of a (scaled) classical autoencoder loss while the last term avoids posterior collapse by penalizing the negative entropy of the variational posterior. While this loss has an interpretable appeal, it is important to keep in mind that it is just a tractable surrogate for the log-likelihood. The gap between the ELBO and log-likelihood can be decomposed into an inference gap and an amortization gap [14]. Large gaps lead to highly sub-optimal training since the network is trained on a loose approximation of the true objective. **Normalizing flows:** The unavailability of a closed form log-likelihood introduces a sub-optimality in VAE training that can only be remedied using complex posterior models or high variance lower bounds. NFs are alternative methods that assume the latent manifold to have the same dimensionality of the ambient space. Consider  $\mathcal{M} = \mathbb{R}^N$  and  $\phi(y; \theta)$  being an invertible differentiable mapping. Under these assumptions, the log-likelihood of the model can be expressed in closed form using the change-of-variable formula  $\log p(x) = \log p_0(\phi^{-1}(y)) + \log |\det D\phi^{-1}(y)|$ , where  $D\phi^{-1}(y)$  is the Jacobi matrix of the inverse mapping. If the base distribution is standard normal, the loss has the form

$$\mathcal{L}_{\text{NF}}(\theta) = \frac{1}{2} (\phi^{-1}(x; \theta))^2 + \log |\det D\phi^{-1}(x; \theta)|. \quad (3)$$

NF architectures are designed by composing  $K$  invertible layers  $\phi_k$ . Affine layers divide the variables in two blocks  $y_k^1$  and  $y_k^2$ , one of which remain unchanged and the other is scaled and translated based on the first  $\phi_k(y_k^2) = y_{k+1}^2 = s(y_k^1) \odot y_k^2 + m(y_k^1)$ , where  $s$  is an arbitrary positive-valued function and  $m$  is an unconstrained function. When applied in the inverse direction, this layer becomes  $(y_{k+1}^2 - m(y_{k+1}^1))/s(y_k^1)$ , which "predicts away" the mean and variance of one block given the other. Using several of these layers with randomized partitions gradually removes statistical dependencies until at the last layer the resulting  $y$  variable approximately matches the uncorrelated Gaussian target  $p_0$ . **Rectangular and injective flows:** Using  $\mathcal{M} = \mathbb{R}^N$  results in models that do not offer a coordinate system for a lower dimensional signal manifold and do not have a clear separation between signal space and residual noise. Injective flows (IFs) relax the invertibility constraint of NFs by allowing for a lower dimensional signal manifold  $\mathcal{M} = \mathbb{R}^D$ . This results in a model where the likelihood is only defined along the signal space and therefore cannot be expressed as a probability density. However, if the mapping  $\phi(y; \theta)$  is injective, the on-manifold density  $p_{\mathcal{M}}(\phi(z); \theta)$  exists and it is tractable for some choice of architecture [6, 15, 45, 43, 13]. This function can be extended to off-manifold data-points by applying a pseudo-inverse, i.e. by projecting the data on the manifold itself prior to the evaluation. Unfortunately, the resulting log-likelihood can only be used to train the on-manifold density but cannot train the embedded manifold itself towards the data. In this sense, IFs cannot be directly used for manifold learning. A solution is to add an ad-hoc "autoencoder term" that penalizes the distance of the datapoints from the manifold. This results in the following loss

$$\mathcal{L}_{\text{IF}}(\theta) = -\log p_{\mathcal{M}}(\mathcal{P}_{\mathcal{M}}(x, \theta); \theta) + \beta \|x - \mathcal{P}_{\mathcal{M}}(x, \theta)\|_2^2, \quad (4)$$

where  $\mathcal{P}_{\mathcal{M}}$  projects the data on the embedded manifold and  $\beta$  is a free parameter that needs to be independently calibrated. This latter term is reminiscent of the reconstruction error loss of an

autoencoder, but it does not follow from a log-likelihood and has a free hyper-parameter. Tractability of pseudo-inverse and Jacobian factors can be achieved by imposing rather strict constrictions on the mapping architecture [9, 64].

### 3 Autoencoding with normalizing flows

We are finally ready to introduce our contribution, where we will show that autoencoders can be seen as a special class of NFs. Autoencoders work by mapping the data into a (often low dimensional) latent representation, which is then used to predict the original variables. Here, we will outline how this can be done using invertible layers. Like most things in the NF literature, our derivation starts with a partition of the variables into two blocks  $x^{1:D}$  and  $x^{D:N}$ . We refer to  $x^{1:D}$  as core variables while we refer to  $x^{D:N}$  as shell variables. We assume the core space to be  $D$ -dimensional and the shell space  $N - D$ -dimensional. For now we assume that the dimensionality  $D$  of the signal space is smaller than the ambient dimension  $N$ . We will consider the  $D > N$  case, which is common in some modern VAE approaches, in a later section by appropriately expanding the ambient space. As in regular autoencoders, all variables are encoded in a latent  $z$ . However, in order to ensure invertibility, this encoding has to have a special form. The simplest option is to use an affine layer:

$$z_1 = g_m(x^{D:N}; \theta) + g_\sigma(x^{D:N}; \theta) \odot n_1^{-1}(x^{1:D}; \theta), \quad (5)$$

where  $g_m$  and  $g_\sigma$  are the mean and scale output channels of a conventional encoder architecture taking a masked input and  $n_1^{-1}$  is a flow architecture, which we refer to as the *core encoder*. It is insightful to notice that Eq. 5 is identical to the reparameterization formula of VAEs (Eq.1) but with a masked encoder and the noise replaced by a transformation of a block of the input variables. We can now use  $z$  to define the deviations between the data and the autoencoder predictions. However, in order to ensure invertibility, we can only model the deviations of the shell variables  $x^{D:N}$ , since all the statistical variability in the core variables is encapsulated in the latents  $z_1$ . This can be done using a conventional decoder architecture in an affine layer:

$$\delta^{D:N} = \frac{x^{D:N} - f_m^{D:N}(z_1; \theta)}{f_\sigma^{D:N}(z_1; \theta)}, \quad (6)$$

where  $f^{D:N}$  denotes the shell outputs of a conventional decoder architecture. Like in VAEs, we can assume that these normalized deviations follow a standard normal distribution  $\delta^{D:N} \sim \mathcal{N}(0, I)$ . This implies that  $\delta$  can be seen as a block of transformed variables, exactly like the latents in a regular NF. However, the deviations  $\delta^{D:N}$  are not latent variables in the usual sense of the term since they do not have expressive power beyond white noise modeling. This realization is the key to circumvent the invertibility constraint and thereby to define a fully invertible model with  $D < N$  "proper" latent variables.

The remaining "normalized" variables can be obtained by applying an additional arbitrary flow transformation to the latents:  $z_0 = n_0^{-1}(z_1; \theta) \sim \mathcal{N}(0, 1)$ . We refer to  $n_0$  as the *prior flow*, since it corresponds to the prior distribution in a VAE. Strictly speaking, like in VAEs, this prior does not need to be a flow and can be an arbitrary differentiable probabilistic model. Altogether, these transformations define a normalizing flow  $\Phi^{-1}(x^{1:D}, x^{D:N}) = z_0, \delta^{D:N}$ . Strikingly, the (negative) log-likelihood of this flow resembles an autoencoder loss:

$$\log p(x; \theta) = \underbrace{\frac{1}{2} \left\| b \odot \frac{x - f_m(z_1(x; \theta); \theta)}{f_\sigma(z_1(x; \theta); \theta)} \right\|_2^2}_{\text{Masked reconstruction error}} + \underbrace{\frac{1}{2} \|z_0(x; \theta)\|_2^2}_{\text{Latent shrinkage}} + \log |\det D\Phi^{-1}(x; \theta)|, \quad (7)$$

where  $b$  is a binary mask with ones corresponding to the shell variables and zeros elsewhere.

#### 3.1 Partition strategies and ambient space expansion

So far, we did not specify how to select core and shell variables. The most straightforward approach is to use an appropriately chosen partition of the original variables. For example, in an image we could extract a central sub-image of "core pixels" and have the image with cropped center as shell. An AEF with this kind of partition interpolates between a regular normalizing flow (for  $D \approx N$ ) and an autoencoder (for  $D \ll N$ ). However, this approach limits the number of latents to be smaller than



$N$  and reduces compatibility with the VAE literature. Furthermore, in the case of noise corrupted data this partitioning strategy does not allow for denoising of the core variables since they do not have corresponding deviations. All these issues can be circumvented if we appropriately expand the ambient space. Consider a parameterized injective function  $\Psi : \mathbb{R}^N \rightarrow \mathbb{R}^{N+D}$ , defined as follows  $\Psi(x; \gamma) = (x, w = h(x; \gamma))$ , where  $\gamma$  are the transformation parameters. This function expands the ambient dimensionality but, since the transformation is injective and deterministic, it leaves the dimensionality of the signal manifold unchanged. Conceptually, this should be seen as a form of pre-processing feature expansion and not an architectural component of a flow. In this expanded space, we can define deviations for all the original variables and, consequently, use a loss with VAE-style reconstruction error on all variables. This can be done simply by using a regular AEF architecture with the original variables  $x$  as shell and  $w = h(x)$  as core. This results in the following encoding layer:

$$z_1 = g_m(x; \theta) + g_\sigma(x; \theta) \odot n_1^{-1}(h(x; \gamma); \theta). \quad (8)$$

Note that this differs from the well-known VAE reparameterized encoding formula just by the fact that the input white noise is replaced by a deterministic function of the data. This is the only architectural difference between VAEs and AEF in the extended space (See Fig. 1c). In fact, even the core encoder  $n_1^{-1}$  is analogous to a posterior flow transformation in a VAE, which in that case acts on input noise. Similarly, the decoder now can work without masking and is therefore identical to VAE decoders. It is not immediately obvious that the feature expansion parameters  $\gamma$  can be trained by maximizing the log-likelihood. However, this joint training can be fully justified as the minimization of (the limit of) KL divergences (see Appendix A), which results in the following objective function:

$$\begin{aligned} \mathcal{L}_{\text{AEF}}(\theta, \gamma) = & \underbrace{\frac{1}{2} \left\| \frac{x - f_m(z_1(x, h(x; \gamma); \theta); \theta)}{f_\sigma(z_1(x, h(x; \gamma); \theta); \theta)} \right\|_2^2}_{\text{Reconstruction error}} + \underbrace{\frac{1}{2} \|z_0(x, h(x; \gamma); \theta)\|_2^2}_{\text{Latent shrinkage}} \\ & + \log |\det D\Phi^{-1}(x, h(x; \gamma); \theta)|, \end{aligned} \quad (9)$$

which is just the log-likelihood in the expanded ambient space. The main difference with respect to the VAE loss in Eq. 2 is the removal of the stochastic sampling and the replacement of the posterior entropy term with an appropriate Jacobian determinant. We include the pseudocode for computing the objective function as negative log likelihood in Algorithm 1. During generative sampling, the additional variables  $w$  are redundant and can be discarded. This implies that, when using this feature expansion strategy, the core flow  $n_1$  does no longer participate in the generative sampling and it instead has an auxiliary role. This is a sign of its strong relation with the posterior flow in a VAE, which is already implicit in Eq. 8. Another similarity with VAEs is the fact that the marginal likelihood of the original variables  $p(x) = \int p(x, w)dw$  cannot be obtained in closed-form from the joint  $p(x, w)$ . We provide an efficient importance sampling scheme in Appendix B. However, this is only needed for evaluation purposes, as no importance sampler or bound needs to be used during training since the exact joint log-likelihood provides the appropriate training loss. In fact, the dimensionality of the ambient space is usually largely arbitrary, depending on factors such as the sampling resolution of cameras and digital microphones instead of the physical features of their respective measured signals. In the next section, we will show that the effective dimensionality of the flow can be reduced by maximum likelihood training.

### 3.2 Manifold learning and dimensionality reduction

In this section, we will consider the noiseless case where the true data is generated from a  $D$ -dimensional manifold with euclidean topology:  $D = \{x = \phi(y) \mid y \in \mathbb{R}^D\}$ , where  $\phi$  is a smooth injective mapping. Since  $\phi$  is injective, there exists an on-manifold inverse  $\psi^\dagger(\psi(y)) = y$ , which takes embedded data as input and returns its  $D$ -dimensional parameterization. This implies that, given powerful enough encoder and decoder architectures, it is always possible to find a latent embedding  $z_1 \in \mathbb{R}^D$  that gives perfect reconstructions. In a AEF architecture, this implies that the shell variables can be entirely "predicted away":  $\delta \propto x - f_m(z_1; \theta) = 0$ , where, as explained in the previous section, we assumed the use of  $x \in \mathbb{R}^N$  as shell and  $w = h(x) \in \mathbb{R}^D$  as core. If the network achieves this state of perfect decoding, the training signal for  $f_m$  vanishes while the training loss for  $f_\sigma$  is given by the Jacobian term  $-\log f_\sigma(z_1, \theta)$ , which is minimized when  $f_\sigma \rightarrow 0$ . This behavior introduces a logarithmic divergence since, at the limit, the likelihood is a singular probability measure of the form:  $p(z_1, x) = \delta_{\text{Dirac}}(x - f_m(z_1; \theta))p(z_1)$ . However, as far as  $f_\theta$  is independently parameterized, this

---

**Algorithm 1** Negative Log Likelihood AEF on expanded ambient space:  $g$ : Encoder;  $f$ : Decoder;  $h$ : feature expansion map;  $n_1$ : core encoder;  $n_0$ : prior flow;  $\theta$ : model parameters,  $\gamma$ : feature expansion parameters;  $x$ : input image

---

```

procedure NEGATIVELOGLIKELIHOOD( $x$ )
   $\log |\det J| \leftarrow 0$ 
   $w \leftarrow h(x; \gamma)$ 
   $z_1 \leftarrow g_m(x; \theta) + g_\sigma(x; \theta) \odot n_1^{-1}(w; \theta)$ 
   $\log |\det J| \leftarrow \log |\det J| + \log |\det J(n_1^{-1}(w; \theta))| + \sum \log g_\sigma(x; \theta)$ 
   $\delta \leftarrow \frac{x - f_m(z_1; \theta)}{f_\sigma(z_1; \theta)}$ 
   $\log |\det J| \leftarrow \log |\det J| - \sum \log f_\sigma(z_1; \theta)$ 
   $z_0 \leftarrow n_0^{-1}(z_1; \theta)$ 
   $\log |\det J| \leftarrow \log |\det J| + \log |\det J(n_0^{-1}(z_1; \theta))|$ 
  return  $-(\sum \mathcal{N}(z_0; 0, 1) + \sum \mathcal{N}(\delta; 0, 1) + \log |\det J|)$ 

```

---

infinity does not affect the gradients in the other parts of the network. Therefore, AEFs can be used for manifold learning and dimensionality reduction even if the likelihood is not defined in that limit.

### 3.3 Noiseless sampling and the noiseless rectangular flow

After training, whether or not the shell variables have been predicted away exactly, we can extract a rectangular flow  $\tilde{\Phi} : \mathbb{R}^D \rightarrow \mathbb{R}^N$  from the invertible architecture  $\Phi$ :

$$\tilde{\Phi}(z_0) = \Phi^{1:N}(z_0, 0). \quad (10)$$

This is a formalization of the noiseless sampling commonly used in VAEs. Note that this rectangular flow is trained solely by maximum likelihood without the additional ad-hoc losses used in the injective flow literature to "push" the range toward the signal manifold.

## 4 Related Work

**Improvements of VAE training:** In recent years, there have been many works analyzing and improving the training procedure of VAEs. Works such as [33], [77] and [1] diagnose some issues with ELBO training and propose a series of methods to improve results. [62] and [16], propose an augmented objective to tackle specific optimization issues. On the same vein, [14] and [49] offer a theoretical analysis of the factors affecting the quality of approximate inference in VAEs and introduce strategies to alleviate them. None of these works introduce an exact maximum likelihood training. A popular way to improve VAEs is to use a more flexible prior or posterior distribution. [59] and [40] use NFs as variational posteriors, showing how the aggregate posterior matches the prior more closely, while [68] uses a variational mixture of posteriors as prior. [50] uses a two-stage training procedure, in which first they train a VAE with a NF prior, and then combine the decoder with Glow [39] for improved sample quality. An alternative line of research is the use of hierarchical priors with several stochastic layers [67, 47]. More recent works use hierarchical VAEs with many layers, achieving state of the art log-likelihood and generating images with impressive sample quality [69, 10, 32]. These works use a latent dimensionality that is greater, often by orders of magnitude, than the dimensionality of the ambient space. This dimensionality expansion greatly ameliorate the problem of posterior separations diagnosed in [16] at the price of higher computational and memory costs and lower interpretability. Interestingly, a recent post-training analysis showed that just a few percents of the hierarchical VAE's latent dimensions are needed to encode the data [32]. **Stochastic auxiliary variables and augmented normalizing flows:** The fact that VAE encoding can be seen as a form of affine coupling was first noticed in [18] (Appendix C). This allows to conceptualize the one-sample reparameterization estimate of the ELBO as a likelihood in a stochastically augmented space. However, this is just an equivalent re-formulation and does not solve the inference sub-optimality problems of VAEs, which in this setting can be explained by the fact that sharp posteriors correspond to singular points of non-invertibility. The approach was recently generalized in [27], where several VAE-style affine layers are stacked in a flow architecture that takes noise augmented input. The stacking procedure removes the signal/noise separation and autoencoder-like loss of

VAEs since the final prediction is not compared with the original image but only with the previous layer. The resulting model is very similar to other auxiliary-augmented flows [12, 74, 8]. **Two-steps training procedures:** A recent trend in generative modeling is to disentangle the tasks of learning a low-dimensional latent representation and maximum-likelihood density estimation. [16] proposes a two-stage procedure for training VAEs, and show its effectiveness both theoretically and empirically. [24] propose to instead use an explicit regularization scheme for the decoder, and employ an ex-post density estimation on the latent space to allow for sampling and ensure that the latent space is distributed according to a simple distribution. Similarly, [76] and [5] use a deterministic autoencoder to learn the latent representation of the data, and a normalizing flow to model the distribution of such latents, leading to better density estimation while avoiding over-regularization of the latent variables. More recently, [46] discusses the problem of manifold overfitting, which arises when the manifold is learned but not the distribution on it, and propose a two-step training procedure applicable to all the likelihood-based models. **NFs on manifolds:** Several authors propose variations of NFs that can model data on a manifold. Works such as [22], [48] and [61] assume that the dimensionality reducing map is already known and available. [37, 34] propose methods based on adding noise to the data, which are capable of learning unknown lower-dimensional manifolds. Injective flows strive for the same goal by using injective deterministic transformations to map the data to a lower dimensional base density. [6], [43] and [13] train injective flows with a two-steps training procedure in which they alternate manifold and density training, while [45] introduces lower bounds on the injective change of variable. [15] combines injective flows with an additive noise model to account for deviations from the learned manifold using stochastic inversions trained on a variational bound. In [9] the authors train injective flows by evaluating the in-manifold likelihood using a modification of the change of variable formulas for rectangular Jacobi matrices, which is then supplemented by an additional ad-hoc reconstruction loss. [64] uses conformal embeddings to train injective flows with exact on-manifold log-likelihood plus an additional *ad hoc* reconstruction loss.

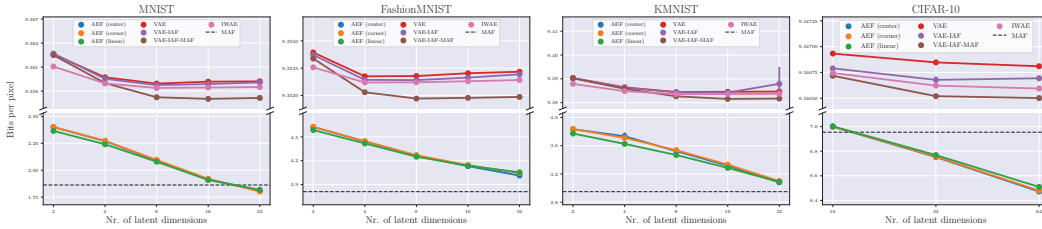


Figure 2: Mean and 95% confidence interval (based on 5 runs) of BPP scores as function of the latent dimensionality.

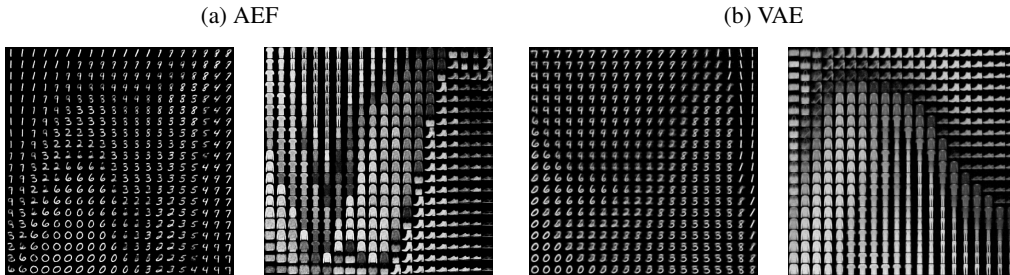


Figure 3: Visualization of learned 2d manifolds for AEF (MLE) and architecturally equivalent VAE (ELBO) trained on MNIST and FashionMNIST with a two-dimensional latent space.

## 5 Experiments

We now show empirically that the exact maximum likelihood training leads to drastically improved results compared to architecturally equivalent VAEs. Our aim is to show the difference in performance between exact log-likelihood and ELBO objective functions when the architecture is kept constant. Therefore, in our VAE baselines we do not use the many regularization, annealing and KL scaling terms that are common in VAE applications [69, 10]. However, we make sure to compare

architecturally identical models with strong prior and variational posteriors, which in themselves ameliorate some of the pathologies of the ELBO [40, 68]. As baselines, we use the original VAE algorithm as introduced in [41], the Importance Weighted Autoencoders (IWAE) [7], a VAE with Inverse Autoregressive Flow posterior (VAE-IAF) [40], and a variant which also uses a Masked Autoregressive Flow (MAF) [53] as prior (VAE-IAF-MAF). This latter model is the main comparison as it is architecturally identical to our AEF. We compare the baselines against three versions of AEF: two in which we select either the center pixels or the corner pixels as core variables, referred to as *center* and *corner* respectively, and one in which we use the extended ambient space with linear features, which we refer to as *linear*. More details about the experiments and results can be found in Appendix C and D. The code for all the experiments is available at: <https://github.com/gisilvs/AEF>.

**Manifold learning:** Autoencoders are ideal tools to extract interpretable low dimensional signal manifolds embedded in much higher dimensional ambient spaces. In these experiments, we investigate quantitatively and qualitatively the manifold learning capabilities of AEFs and VAEs. We shall focus on four relatively small scale datasets: MNIST, FashionMNIST, KMNIST and CIFAR10 [17, 75, 11, 44]. To keep things simple, we use small conventional encoder and decoder architectures and masked autoregressive flows as prior and core encoder (see Appendix C.1). Fig. 3 shows the learned manifold with two-dimensional latent space. We report the quantitative results in terms of bits per pixels (BPP) as function of the latent dimensionality in Fig. 2. AEF-based models achieve strikingly lower BPP values compared to the VAEs baselines, and, for higher numbers of latent dimensions, often achieve superior BPP performance than the non-dimensionality reducing normalizing flow (MAF). Importantly, the deterministic dimensionality expansion of AEF-linear did not introduced any discernible gap in the likelihood when compared with the other AEF models. Additional plots and comparison of FID score are reported in D.1. All AEF models achieve much higher sample quality than all baselines, including MAF. AEF samples are visually sharp even for low-dimensional latent spaces (see Fig.3, Fig. 4 and Appendix D.1). On the other hand, VAE samples are blurry and often superimpose exemplars of two classes in the same image.

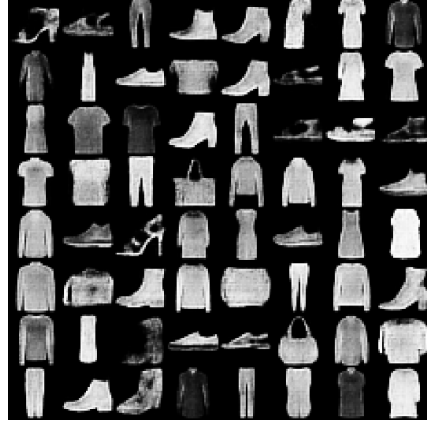


Figure 4: Samples from AEF-linear trained on FashionMNIST with a latent dimensionality of 32.

**Denoising:** Denoising is one of the main applications of the classical autoencoder literature. The basic idea is that the signal can be compressed in a low dimensional manifold while the (white) noise, being incomprehensible, is filtered out. The denoising problem shows the capacity of our training scheme to separate the signal and the noise spaces, thereby performing an adaptive non-linear filtering. We test performance on the MNIST, FashionMNIST and KMNIST datasets with different noise levels and we compare against architecturally equivalent VAEs and least squares denoising autoencoders (AE). All models were trained exclusively on noisy data. We report the MSE reconstruction error for the high noise regime ( $\sigma = 0.75$ ) and latent space of size 32 in Table 1. Results obtained with lower latent size dimension and lower noise are reported in Appendix D.2. AEFs achieve better reconstructions, as can be easily confirmed by inspecting the denoised images shown in Fig. 5. The sharpness of the reconstructions is surprising as the models were only trained on highly corrupted images, a clear sign of the performance of the signal/noise separation scheme.

	MNIST	FashionMNIST	KMNIST
VAE (IAF-MAF)	$0.111 \pm 1.15e - 04$	$0.075 \pm 1.05e - 04$	$0.130 \pm 1.77e - 04$
AE	$0.080 \pm 3.84e - 04$	$0.062 \pm 4.41e - 05$	$0.089 \pm 1.48e - 04$
IAE (linear)	<b><math>0.036 \pm 3.59e - 04</math></b>	<b><math>0.043 \pm 4.36e - 04</math></b>	<b><math>0.073 \pm 2.53e - 04</math></b>

Table 1: Mean squared error between reconstructions of noisy inputs and original inputs in the high noise regime, where the standard deviation of the noise distribution is equal to 0.75. All the models have a latent dimensionality of 32. We report mean and standard error of the mean over five runs.

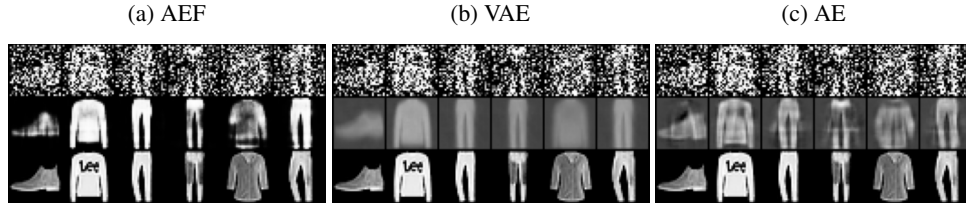


Figure 5: Examples of reconstruction performance of AEF, VAE with IAF posterior and MAF prior, and deterministic autoencoder (AE) trained on samples in the high noise regime ( $\sigma = 0.75$ ) and a latent dimensionality of 32. **Top**: image with added noise; **Middle**: reconstructed image; **Bottom**: original image.

**Generative modeling:** In this final experiment, we probe the generative performance of AEFs in CelebA-HQ (resized to  $32 \times 32$ ), a more complex naturalistic dataset [35]. We focus again on models with significantly less latent variables than observable dimensions since this is the regime that is the most problematic for traditional VAE training. We use a more complex Encoder-Decoder architecture with residual blocks, similar to the one used in [10], and compare the performances of AEF-linear and its architecturally identical VAE (MAF prior, IAF posterior) for different latent dimensions. Table 2 shows that AEFs significantly outperform VAEs both in terms of bits per pixels and FID score. AEF is capable of generating significantly sharper and more detailed samples (Fig. 6), while also being able to faithfully reconstruct given input images (Fig. 1).

		Nr. of latent dimensions		
Models		64	128	256
VAE	BPP	9.348	9.347	9.346
	FID	127.50	117.39	105.97
AEF	BPP	<b>6.210</b>	<b>5.877</b>	<b>5.527</b>
	FID	<b>52.60</b>	<b>36.23</b>	<b>27.85</b>

Table 2: Bits per pixel and Frechet Inception Distance for AEF and VAE models trained on CelebA-HQ averaged over two runs. Lower is better for both metrics.

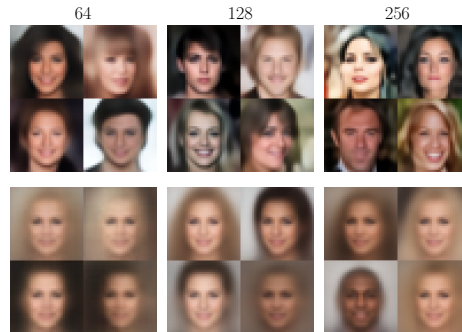


Figure 6: Samples from an AEF (top row) and VAE (bottom row) trained on rescaled CelebA-HQ with 64, 128, and 256 latent dimensions respectively.

## 6 Discussion and conclusions

In this work we showed that autoencoders, if properly constructed out of invertible layers, can be trained by maximum likelihood. This results in a log-likelihood objective function that can be directly used in the training of any pre-existing VAE and VAE-like model that uses Gaussian residual noise. In our experiments, we showed that this new training approach greatly improves performance while solving most of the instabilities intrinsic in ELBO training. When compared to VAEs, the main limitation of AEFs is that they cannot straightforwardly use discrete emission models (decoders) since their flow architecture is assumed to work on continuous data. Another limitation is that, since we are not using stochastic auxiliary variables, AEFs have the same topological constraints of regular NFs [12, 8]. Our work opens the door to hybrid autoencoder-flow models that can learn how to reduce the latent dimensionality by "predicting away" some dimensions, possibly at several different stages of processing. Adding manifold learning capabilities to NF has great potential since it can avoid some of the pathologies of invertible models when used on lower dimensional data, while at the same time increasing training efficiency.

## Acknowledgements

OnePlanet Research Center acknowledges the support of the Province of Gelderland.

## References

- [1] A. Alemi, B. Poole, I. Fischer, J. Dillon, R. A. Saurous, and K. Murphy. Fixing a broken ELBO. *International Conference on Machine Learning*, 2018.
- [2] R. Bamler, C. Zhang, M. Opper, and S. Mandt. Perturbative black box variational inference. *Advances in Neural Information Processing Systems*, 2017.
- [3] Y. Bengio, A. Courville, and P. Vincent. Representation learning: A review and new perspectives. *IEEE transactions on pattern analysis and machine intelligence*, 35(8):1798–1828, 2013.
- [4] L. Biewald. Experiment tracking with weights and biases, 2020. Software available from wandb.com.
- [5] V. Böhm and U. Seljak. Probabilistic auto-encoder. *arXiv preprint arXiv:2006.05479*, 2020.
- [6] J. Brehmer and K. Cranmer. Flows for simultaneous manifold learning and density estimation. *Advances in Neural Information Processing Systems*, 2020.
- [7] Y. Burda, R. Grosse, and R. Salakhutdinov. Importance weighted autoencoders. *arXiv preprint arXiv:1509.00519*, 2015.
- [8] A. Caterini, R. Cornish, D. Sejdinovic, and A. Doucet. Variational inference with continuously-indexed normalizing flows. *Uncertainty in Artificial Intelligence*, 2021.
- [9] A. L. Caterini, G. Loaiza-Ganem, G. Pleiss, and J. P. Cunningham. Rectangular flows for manifold learning. *Advances in Neural Information Processing Systems*, 2021.
- [10] R. Child. Very deep vaes generalize autoregressive models and can outperform them on images. *International Conference on Learning Representations*, 2021.
- [11] T. Clauwat, M. Bober-Irizar, A. Kitamoto, A. Lamb, K. Yamamoto, and D. Ha. Deep learning for classical japanese literature. *arXiv preprint arXiv:1812.01718*, 2018.
- [12] R. Cornish, A. Caterini, G. Deligiannidis, and A. Doucet. Relaxing bijectivity constraints with continuously indexed normalising flows. *International conference on machine learning*, 2020.
- [13] E. Cramer, F. Rauh, A. Mitsos, R. Tempone, and M. Dahmen. Nonlinear isometric manifold learning for injective normalizing flows. *arXiv preprint arXiv:2203.03934*, 2022.
- [14] C. Cremer, X. Li, and D. Duvenaud. Inference suboptimality in variational autoencoders. *International Conference on Machine Learning*, 2018.
- [15] E. Cunningham, R. Zabounidis, A. Agrawal, I. Fiterau, and D. Sheldon. Normalizing flows across dimensions. *arXiv preprint arXiv:2006.13070*, 2020.
- [16] B. Dai and D. Wipf. Diagnosing and enhancing vae models. *International Conference on Learning Representations*, 2019.
- [17] L. Deng. The mnist database of handwritten digit images for machine learning research. *IEEE Signal Processing Magazine*, 29(6):141–142, 2012.
- [18] L. Dinh, D. Krueger, and Y. Bengio. Nice: Non-linear independent components estimation. *arXiv preprint arXiv:1410.8516*, 2014.
- [19] L. Dinh, J. Sohl-Dickstein, and S. Bengio. Density estimation using real nvp. *International Conference on Learning Representations*, 2017.
- [20] C. Durkan, A. Bekasov, I. Murray, and G. Papamakarios. nflows: normalizing flows in PyTorch, Nov. 2020.
- [21] C. F., S. M., and H. N. Testing the manifold hypothesis. *Journal of the American Mathematical Society*, 29(4):983–1049, 2016.
- [22] M. C. Gemicci, D. Rezende, and S. Mohamed. Normalizing flows on riemannian manifolds. *arXiv preprint arXiv:1611.02304*, 2016.
- [23] M. Germain, K. Gregor, I. Murray, and H. Larochelle. Made: Masked autoencoder for distribution estimation. *International Conference on Machine Learning*, 2015.

- [24] P. Ghosh, M. S. Sajjadi, A. Vergari, M. Black, and B. Schölkopf. From variational to deterministic autoencoders. *International Conference on Learning Representations*, 2020.
- [25] I. Goodfellow, J. Pouget-Abadie, M. Mirza, B. Xu, D. Warde-Farley, S. Ozair, A. Courville, and Y. Bengio. Generative adversarial nets. *Advances in neural information processing systems*, 2014.
- [26] K. Gregor, D. Jimenez Rezende, F. Besse, Y. Wu, H. Merzic, and A. van den Oord. Shaping belief states with generative environment models for rl. *Advances in Neural Information Processing Systems*, 2019.
- [27] C.-W. H., L. D., and A. C. Augmented normalizing flows: Bridging the gap between generative flows and latent variable models. *arXiv preprint arXiv:2002.07101*, 2020.
- [28] D. Ha and J. Schmidhuber. Recurrent world models facilitate policy evolution. *Advances in neural information processing systems*, 2018.
- [29] D. Ha and J. Schmidhuber. World models. *arXiv preprint arXiv:1803.10122*, 2018.
- [30] D. Hafner, T. Lillicrap, J. Ba, and M. Norouzi. Dream to control: Learning behaviors by latent imagination. *International Conference on Learning Representations*, 2020.
- [31] D. Hafner, T. Lillicrap, M. Norouzi, and J. Ba. Mastering atari with discrete world models. *International Conference on Learning Representations*, 2021.
- [32] L. Hazami, R. Mama, and R. Thuraiatnam. Efficient-ldvae: Less is more. *arXiv preprint arXiv:2203.13751*, 2022.
- [33] M. D. Hoffman and M. J. Johnson. Elbo surgery: yet another way to carve up the variational evidence lower bound. In *Workshop in Advances in Approximate Bayesian Inference, NIPS*, 2016.
- [34] C. Horvat and J.-P. Pfister. Denoising normalizing flow. *Advances in Neural Information Processing Systems*, 2021.
- [35] T. Karras, T. Aila, S. Laine, and J. Lehtinen. Progressive growing of gans for improved quality, stability, and variation. *International Conference on Learning Representations*, 2018.
- [36] T. Karras, S. Laine, M. Aittala, J. Hellsten, J. Lehtinen, and T. Aila. Analyzing and improving the image quality of stylegan. In *Proceedings of the IEEE/CVF conference on computer vision and pattern recognition*, pages 8110–8119, 2020.
- [37] H. Kim, H. Lee, W. H. Kang, J. Y. Lee, and N. S. Kim. Softflow: Probabilistic framework for normalizing flow on manifolds. *Advances in Neural Information Processing Systems*, 2020.
- [38] D. P. Kingma and J. Ba. Adam: A method for stochastic optimization. *International Conference on Learning Representations*, 2015.
- [39] D. P. Kingma and P. Dhariwal. Glow: Generative flow with invertible 1x1 convolutions. *Advances in neural information processing systems*, 2018.
- [40] D. P. Kingma, T. Salimans, R. Jozefowicz, X. Chen, I. Sutskever, and M. Welling. Improved variational inference with inverse autoregressive flow. *Advances in neural information processing systems*, 2016.
- [41] D. P. Kingma and M. Welling. Auto-encoding variational bayes. *International Conference on Learning Representations*, 2014.
- [42] I. Kobyzev, S. J. Prince, and M. A. Brubaker. Normalizing flows: An introduction and review of current methods. *IEEE transactions on pattern analysis and machine intelligence*, 43(11):3964–3979, 2020.
- [43] K. Kothari, A. Khorashadizadeh, M. de Hoop, and I. Dokmanić. Trumpets: Injective flows for inference and inverse problems. *Uncertainty in Artificial Intelligence*, 2021.
- [44] A. Krizhevsky, G. Hinton, et al. Learning multiple layers of features from tiny images. 2009.
- [45] A. Kumar, B. Poole, and K. Murphy. Regularized autoencoders via relaxed injective probability flow. *International Conference on Artificial Intelligence and Statistics*, 2020.
- [46] G. Loaiza-Ganem, B. L. Ross, J. C. Cresswell, and A. L. Caterini. Diagnosing and fixing manifold overfitting in deep generative models. *arXiv preprint arXiv:2204.07172*, 2022.

- [47] L. Maaløe, M. Fraccaro, V. Liévin, and O. Winther. Biva: A very deep hierarchy of latent variables for generative modeling. *Advances in neural information processing systems*, 2019.
- [48] E. Mathieu and M. Nickel. Riemannian continuous normalizing flows. *Advances in Neural Information Processing Systems*, 2020.
- [49] P.-A. Mattei and J. Frellsen. Leveraging the exact likelihood of deep latent variable models. *Advances in Neural Information Processing Systems*, 2018.
- [50] R. Morrow and W.-C. Chiu. Variational autoencoders with normalizing flow decoders. *arXiv preprint arXiv:2004.05617*, 2020.
- [51] A. Q. Nichol and P. Dhariwal. Improved denoising diffusion probabilistic models. *International Conference on Machine Learning*, 2021.
- [52] G. Papamakarios, E. Nalisnick, D. J. Rezende, S. Mohamed, and B. Lakshminarayanan. Normalizing flows for probabilistic modeling and inference. *Journal of Machine Learning Research*, 22(57):1–64, 2021.
- [53] G. Papamakarios, T. Pavlakou, and I. Murray. Masked autoregressive flow for density estimation. *Advances in neural information processing systems*, 2017.
- [54] P. Pope, C. Zhu, A. Abdelkader, M. Goldblum, and T. Goldstein. The intrinsic dimension of images and its impact on learning. *International Conference on Learning Representations*, 2021.
- [55] A. Radford, J. W. Kim, C. Hallacy, A. Ramesh, G. Goh, S. Agarwal, G. Sastry, A. Askell, P. Mishkin, J. Clark, et al. Learning transferable visual models from natural language supervision. *International Conference on Machine Learning*, 2021.
- [56] A. Ramesh, P. Dhariwal, A. Nichol, C. Chu, and M. Chen. Hierarchical text-conditional image generation with clip latents. *arXiv preprint arXiv:2204.06125*, 2022.
- [57] A. Ramesh, M. Pavlov, G. Goh, S. Gray, C. Voss, A. Radford, M. Chen, and I. Sutskever. Zero-shot text-to-image generation. *International Conference on Machine Learning*, 2021.
- [58] A. Razavi, A. Van den Oord, and O. Vinyals. Generating diverse high-fidelity images with vq-vae-2. *Advances in neural information processing systems*, 2019.
- [59] D. Rezende and S. Mohamed. Variational inference with normalizing flows. *International conference on machine learning*, 2015.
- [60] D. J. Rezende, S. Mohamed, and D. Wierstra. Stochastic backpropagation and approximate inference in deep generative models. *International conference on machine learning*, 2014.
- [61] D. J. Rezende, G. Papamakarios, S. Racaniere, M. Albergo, G. Kanwar, P. Shanahan, and K. Cranmer. Normalizing flows on tori and spheres. *International Conference on Machine Learning*, 2020.
- [62] D. J. Rezende and F. Viola. Taming vaes. *arXiv preprint arXiv:1810.00597*, 2018.
- [63] O. Ronneberger, P. Fischer, and T. Brox. U-net: Convolutional networks for biomedical image segmentation. In *International Conference on Medical image computing and computer-assisted intervention*, pages 234–241. Springer, 2015.
- [64] B. Ross and J. Cresswell. Tractable density estimation on learned manifolds with conformal embedding flows. *Advances in Neural Information Processing Systems*, 2021.
- [65] T. Salimans, A. Karpathy, X. Chen, and D. P. Kingma. Pixelcnn++: Improving the pixelcnn with discretized logistic mixture likelihood and other modifications. *International Conference on Learning Representations*, 2017.
- [66] J. Sohl-Dickstein, E. Weiss, N. Maheswaranathan, and S. Ganguli. Deep unsupervised learning using nonequilibrium thermodynamics. *International Conference on Machine Learning*, 2015.
- [67] C. K. Sønderby, T. Raiko, L. Maaløe, S. K. Sønderby, and O. Winther. Ladder variational autoencoders. *Advances in neural information processing systems*, 2016.
- [68] J. Tomczak and M. Welling. Vae with a vampprior. *International Conference on Artificial Intelligence and Statistics*, 2018.
- [69] A. Vahdat and J. Kautz. Nvae: A deep hierarchical variational autoencoder. *Advances in Neural Information Processing Systems*, 2020.



- [70] A. Van den Oord, N. Kalchbrenner, L. Espeholt, O. Vinyals, A. Graves, et al. Conditional image generation with pixelcnn decoders. *Advances in neural information processing systems*, 2016.
- [71] A. Van Den Oord, O. Vinyals, et al. Neural discrete representation learning. *Advances in neural information processing systems*, 2017.
- [72] A. Van Oord, N. Kalchbrenner, and K. Kavukcuoglu. Pixel recurrent neural networks. *International conference on machine learning*, 2016.
- [73] A. Vaswani, N. Shazeer, N. Parmar, J. Uszkoreit, L. Jones, A. N. Gomez, Ł. Kaiser, and I. Polosukhin. Attention is all you need. *Advances in neural information processing systems*, 2017.
- [74] C. Weilbach, B. Beronov, F. Wood, and W. Harvey. Structured conditional continuous normalizing flows for efficient amortized inference in graphical models. *International Conference on Artificial Intelligence and Statistics*, 2020.
- [75] H. Xiao, K. Rasul, and R. Vollgraf. Fashion-mnist: a novel image dataset for benchmarking machine learning algorithms. *arXiv preprint arXiv:1708.07747*, 2017.
- [76] Z. Xiao, Q. Yan, and Y. Amit. Generative latent flow. *arXiv preprint arXiv:1905.10485*, 2019.
- [77] S. Zhao, J. Song, and S. Ermon. Towards deeper understanding of variational autoencoding models. *arXiv preprint arXiv:1702.08658*, 2017.
- [78] L. Zintgraf, K. Shiarlis, M. Igl, S. Schulze, Y. Gal, K. Hofmann, and S. Whiteson. Varibad: A very good method for bayes-adaptive deep rl via meta-learning. *International Conference on Learning Representations*, 2020.

## A Training the expansion parameters $\gamma$

The feature expansion map  $h(x, \gamma)$  is, strictly speaking, not a component of the flow architecture. Therefore, in spite of its intuitive appeal, it is not obvious that we can train  $\gamma$  by minimizing the joint negative log-likelihood. However, this can be fully justified using a limit of KL divergence between two joint distributions.

We will denote the empirical sampling distribution of the dataset as  $d(x)$ . Now consider the joint distribution

$$q_\sigma(x, w) = d(x)\mathcal{N}(h(x, \gamma), I\sigma) \quad (11)$$

It is easy to see that the KL divergence between  $q(x, w)$  and the joint distribution of the generative model  $p(x, w)$  is given by:

$$D_{\text{KL}}(q_\sigma(x, w), p(x, w)) = -\mathbb{E}_{x, \epsilon}[\log p(x, w)] + c, \quad (12)$$

where the constant  $c$  is independent from both  $\theta$  and  $\gamma$ . This happens because the differential entropy of a Gaussian does not depend on its mean.

Therefore, the gradient with respect to  $\gamma$  is

$$\nabla_\gamma D_{\text{KL}}(q_\sigma(x, w), p(x, w)) = -\mathbb{E}_{x, \epsilon}[\nabla_\gamma \log p(x, w)], \quad (13)$$

which is just the gradient of the stochastically augmented joint log-likelihood. We can now notice that, while the KL divergence is not well-defined for  $\sigma \rightarrow 0$ , the limiting gradient is well-defined since the diverging entropy term does not depend on  $\gamma$ . This leads us with the following limiting gradient:

$$\lim_{\sigma \rightarrow 0} \nabla_\gamma D_{\text{KL}}(q_\sigma(x, w), p(x, w)) \quad (14)$$

$$= -\lim_{\sigma \rightarrow 0} \mathbb{E}_{x, \epsilon}[\nabla_\gamma \log p(x, h(x, \gamma) + \sigma \odot \epsilon)] \quad (15)$$

$$= -\mathbb{E}_x[\nabla_\gamma \log p(x, h(x, \gamma))] , \quad (16)$$

which, up to a proportionality constant, is just the gradient of the negative log-likelihood used to train the flow.

## B Importance sampling for linear AEF

After training, if we wish to compute the probability  $p(x)$  for model comparison purposes, we would need to solve the integral  $p(x) = \int p(x, w)dw$ , which cannot be obtained in closed form. However, we can use an importance sampling scheme:

$$p(x) = \int p(x, w)dw = \int \frac{p(x, w)}{q(w)}dw \approx \frac{1}{K} \sum_k \frac{p(x, w_k)}{q(w_k)} \quad (17)$$

To do so, we first compute  $w = h(x; \gamma)$ , then take  $K$  samples from a normal distribution centered in  $w$ :  $w_1, \dots, w_K \sim q(w) = \mathcal{N}(w, \epsilon)$ , where  $\epsilon$  is the approximate posterior scale and needs to be tuned for each model on the validation set. We perform the rest of the computations using  $w_1, \dots, w_K$  instead of  $w$ , and finally compute the probability in Eq. 17. To reduce the variance of the estimator, we additionally use importance weighted sampling:

$$\log p(x) \approx \log \mathbb{E}_{w_1, \dots, w_K \sim q(w)} \left[ \frac{1}{K} \sum_k \frac{p(x, w_k)}{q(w_k)} \right] \quad (18)$$

## C Experiments' details

### C.1 Encoder and Decoder

For the manifold learning and denoising experiments, all the encoders and decoders consist of a two-layers convolutional neural network. The encoder uses  $3 \times 3$  kernels, 64 for the first layer and 128 for the second. Each layer is followed by ReLU activation. Finally, two linear layers map the feature maps to mean and standard deviation of the latent space respectively. Similarly, the decoder first uses a linear layer to increase the dimensionality of the latent samples, and then two transposed convolutional layers with respectively 128 and 64 kernels of size 4. We use two variants for the decoder: one outputs only the mean value of the target image, while the variance is assumed to be fixed and equal to 1, and the other outputs also the standard deviation, as a set of trainable parameters constrained with softplus activation. In all our experiments, AEF uses the latter decoder, while the VAE-like models use the decoder with fixed variance, as we found empirically that it improves the sample quality.

For the generative modeling we use an encoder and decoder with many more layers and residual blocks, an architecture similar to [10]. In particular, we use the same residual bottleneck block, but the encoder does not output activations at intermediate layers, and the decoder processes only the input coming from the previous layer, without stochastic sampling and prior computation. In other words, we reuse the residual bottleneck blocks from [10] to build a "traditional" encoder-decoder architecture, and the outputs of the encoder and decoder are the same as for the manifold learning and denoising experiments. The number of layers and bottleneck size are taken from the hyperparameters that [10] uses for CIFAR-10.

### C.2 Masked Autoregressive Flow

For all of our NFs, we use and adapt implementations from [20]. Our MAF models stack  $K$  MADE autoregressive layers [23], each with 2 residual blocks with  $N$  hidden units. We add ActNorm [39] between each autoregressive layer. IAF is simply the inverse of MAF. When MAF or IAF are used within an autoencoder architecture, whether as prior, posterior or encoder flow, we use  $K = 4$  and  $N = 256$  for manifold learning and denoising, and  $k = 8$  and  $N = 512$  for generative modeling. The baseline MAF used in the manifold learning experiments has  $K = 4$  and  $N = 256$ . In VAE-IAF, we take IAF to have twice as many parameters, to match the number of parameters used in the other models.

### C.3 Preprocessing Layer

For all the AEF-like models, we apply a preprocessing bijective transformation like the one used in [53]:

$$x = \text{logit}(\lambda + (1 - 2\lambda)z) \quad (19)$$

where  $z$  is the input image and  $\lambda$  is a parameter. We use  $\lambda = 1e^{-6}$  for the MNIST-like datasets and  $\lambda = 0.05$  for CIFAR10 and CelebA-HQ. This transformation is then followed by an ActNorm layer.

#### C.4 Datasets and data pre-processing

In all our experiments, we use a dequantized version of the data, in which we first add uniform noise  $u \sim \mathcal{U}(0, 1)$  to the image and then divide by 256. Division by 256 requires an adjustment in the log likelihood, which we take into account when computing the bits per pixel.

For the denoising experiments we add gaussian white noise  $\mathcal{N}(0, \sigma)$  to the samples, with different levels of  $\sigma$  (0.25, 0.5 and 0.75). By varying the standard deviation of the noise distribution we can increase the intensity of the noise. After adding the noise to the images we clip them so that the pixel values stay in their original range.

For CIFAR-10 and CelebA-HQ we apply random left-right flipping whenever an image is loaded into a batch. For all the models we use 10% of the training dataset as validation set, apart from CelebA-HQ for which we use the predefined train-val-test split.

#### C.5 Training procedure

We train all the models for 100k iterations, and we evaluate the test metrics on the iteration that achieved the best validation loss. For CelebA-HQ, we train instead for  $1M$  iterations and do early stopping if the validation does not improve for at least one unit of negative log likelihood for more than  $20k$  iterations. We use gradient clipping if the magnitude of the gradients is bigger than 200. As optimizer we choose ADAM [38] with a learning rate  $1e - 3$  for the MNIST-like datasets on the manifold learning experiments, and  $1e - 4$  for CIFAR-10, denoising experiments and generative modeling. We use batch size 128 for all the experiments but the ones on CelebA-HQ for which we use a batch size of 64.

We use *Weights & Biases* to track all our experiments and store models' checkpoints. [4]

#### C.6 Compute resources

We used AzureML and Google Colab Pro to run all our experiments. All the manifold learning and denoising experiments are run on one GPU NVIDIA m60, while we use one GPU p-40 for the experiments on CelebA-HQ. We train the MAF baseline on CPU-only machines.

#### C.7 Models' parameters

We report the number of parameters used in each model for the different datasets: Table 3 for the models trained on MNIST-like datasets, for manifold learning and denoising; Table 4 for the manifold learning experiments on CIFAR10; Table 5 for the Image Generation experiments.

Models	Nr. of latent dimensions				
	2	4	8	16	32
VAE	250k	288k	363k	514k	815k
IWAE	250k	288k	363k	514k	815k
VAE-IAF	2.37M	2.42M	2.52M	2.71M	3.12M
VAE-IAF-MAF	2.37M	2.42M	2.52M	2.71M	3.12M
AEF	2.37M	2.42M	2.52M	2.71M	3.12M
AEF (linear)	2.37M	2.42M	2.53M	2.73M	3.15M
MAF	3.47M*	-	-	-	-

Table 3: Approximate number of model parameters for all models trained on MNIST-like datasets. \*Since MAF is a normalizing flow, the base distribution has a dimensionality equal to the dimensionality in the data, in this case  $1 \times 28 \times 28 = 784$ .

Models	Nr. of latent dimensions		
	16	32	64
VAE	611k	1.00m	1.79m
IWAE	611k	1.00m	1.79m
VAE-IAF	2.82M	3.31M	4.30M
VAE-IAF-MAF	2.82M	3.31M	4.30M
AEF	2.82M	3.31M	4.30M
AEF (linear)	2.87M	3.41M	4.49M
MAF	10.5M*	-	-

Table 4: Approximate number of model parameters for all models trained on CIFAR-10. \*Since MAF is a normalizing flow, the base distribution has a dimensionality equal to the dimensionality in the data, in this case  $3 \times 32 \times 32 = 3072$ .

Models	Nr. of latent dimensions		
	64	128	256
VAE-IAF-MAF	18.9M	21.9M	31.0M
AEF (linear)	19.1M	22.3M	31.8M

Table 5: Approximate number of model parameters for all models trained on CelebA-HQ rescaled to  $32 \times 32$ .

## D Additional results

### D.1 Manifold Learning

This section provides further results and images detailing the performance of AEF compared to the baselines. In Figure 7 we show the FID score for all models as a function of the number of latent dimensions, while Figure 8 shows the 2D latent space embedding for the different classes of the MNIST dataset. Figures 9, 10, 11 and 12 show samples and reconstructions from AEFs trained on the various datasets. Figure 13 shows samples and reconstructions of a VAE-MAF-IAF for comparison.

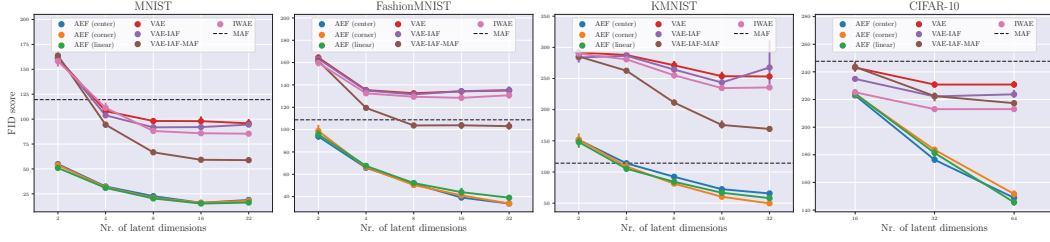


Figure 7: FID score achieved by AEF and the other baselines on multiple datasets. We show the mean and 95% confidence interval based on 5 runs.

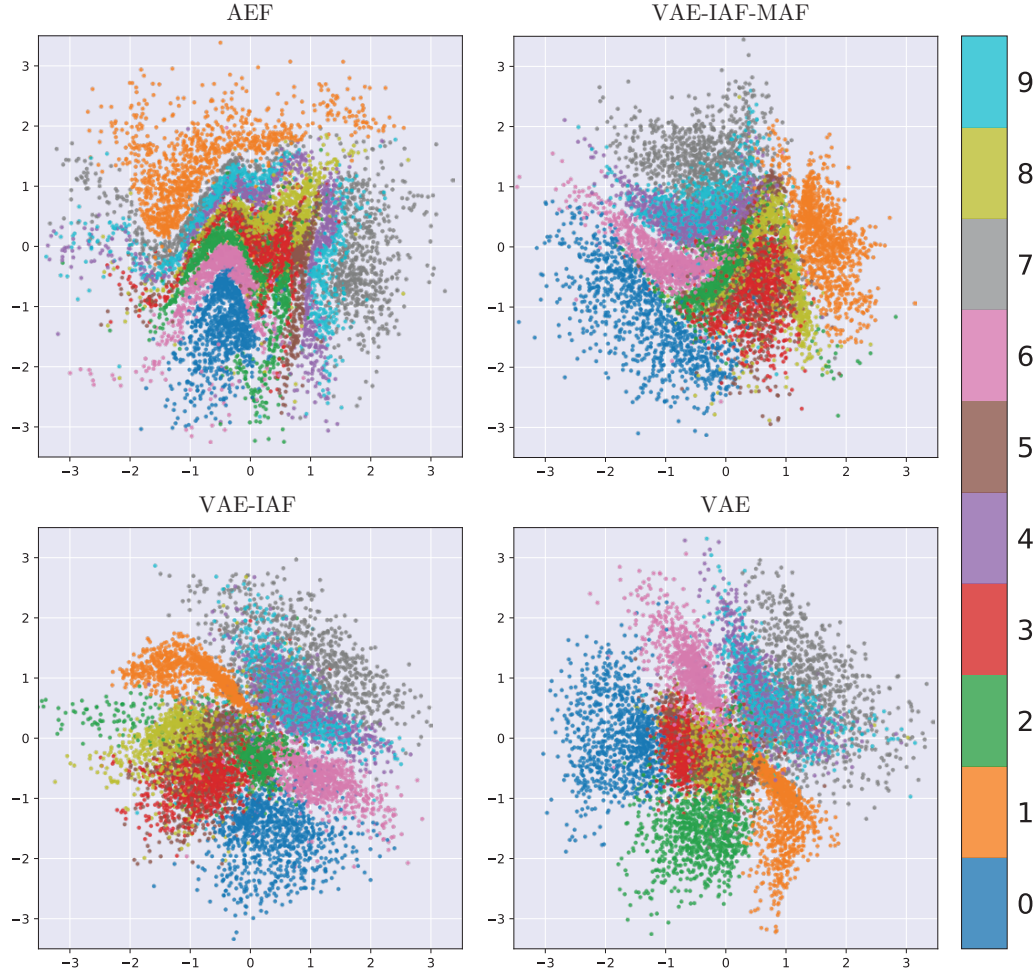


Figure 8: Comparison of 2D latent space embedding for different models on the MNIST dataset.



Figure 9: Samples generated by AEF-linear models trained on MNIST, FashionMNIST, KMNIST and CIFAR-10 with a latent dimensionality of 32 for the MNIST datasets and 64 for CIFAR-10. A temperature of 1.0 was used.

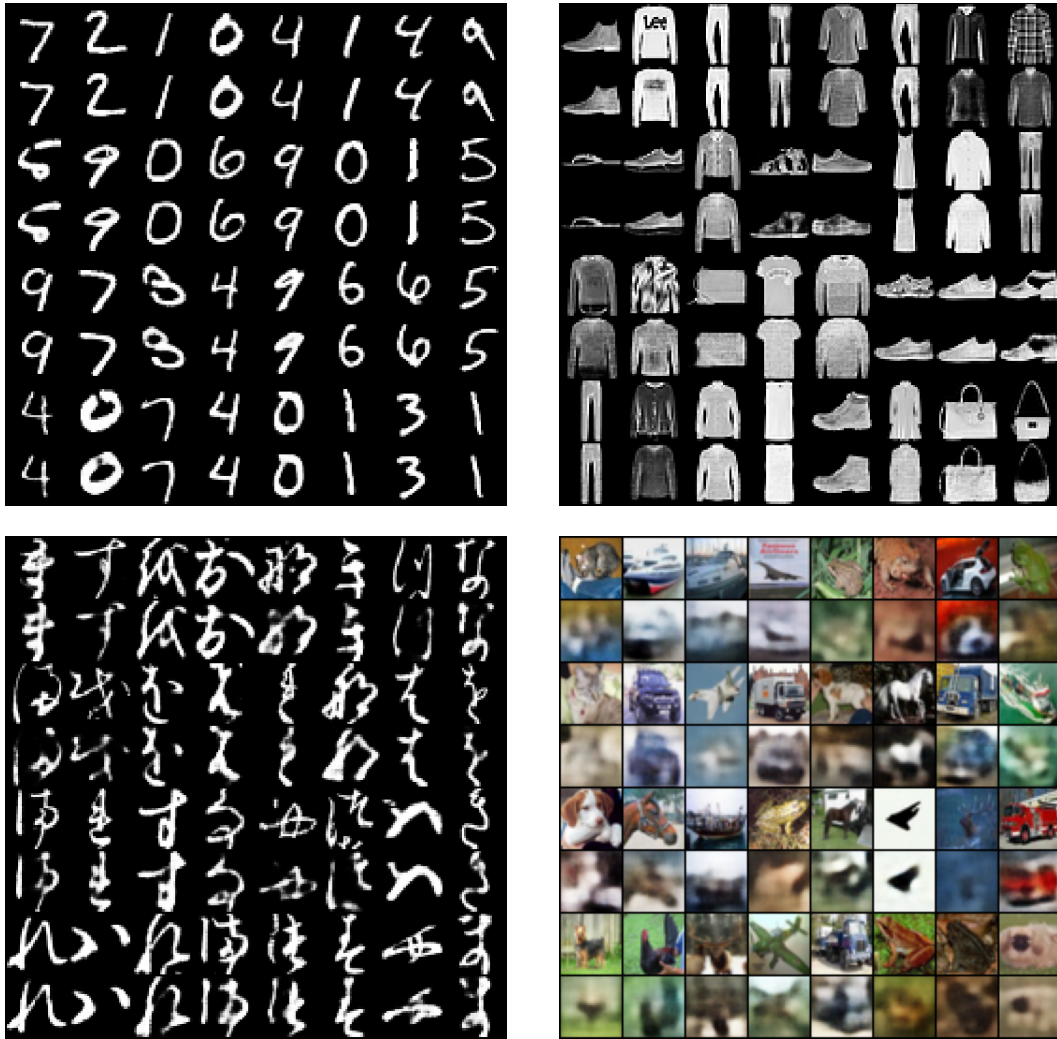


Figure 10: Reconstructions by AEF-linear models trained on MNIST, FashionMNIST, KMNIST and CIFAR-10 with a latent dimensionality of 32 for the MNIST datasets and 64 for CIFAR-10. For each pair the upper row is the original and the lower row the reconstruction.



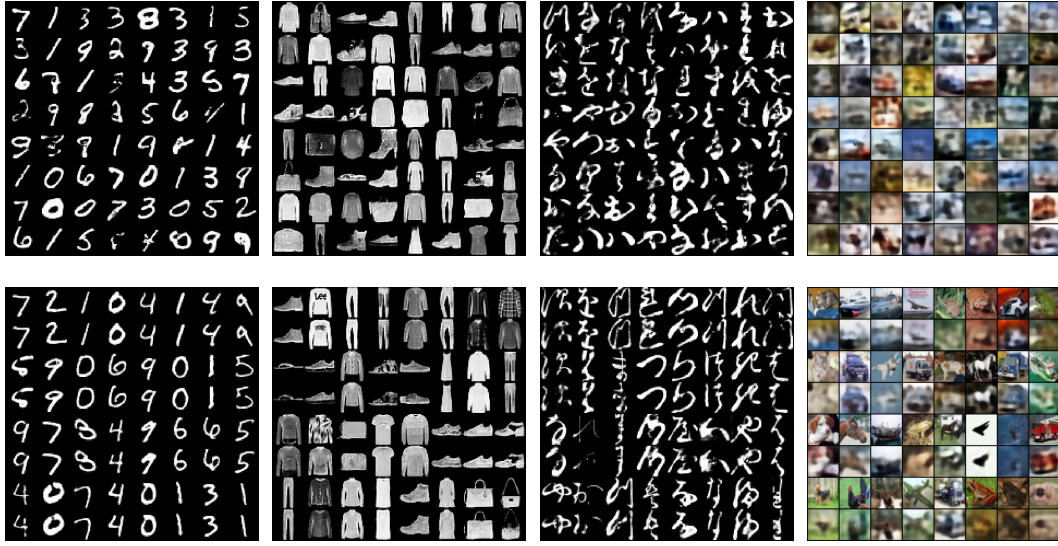


Figure 11: Samples and reconstructions for AEF-center with a latent dimensionality of 32 for the MNIST datasets, and 64 for CIFAR. One can notice artifacts in the center of the samples.

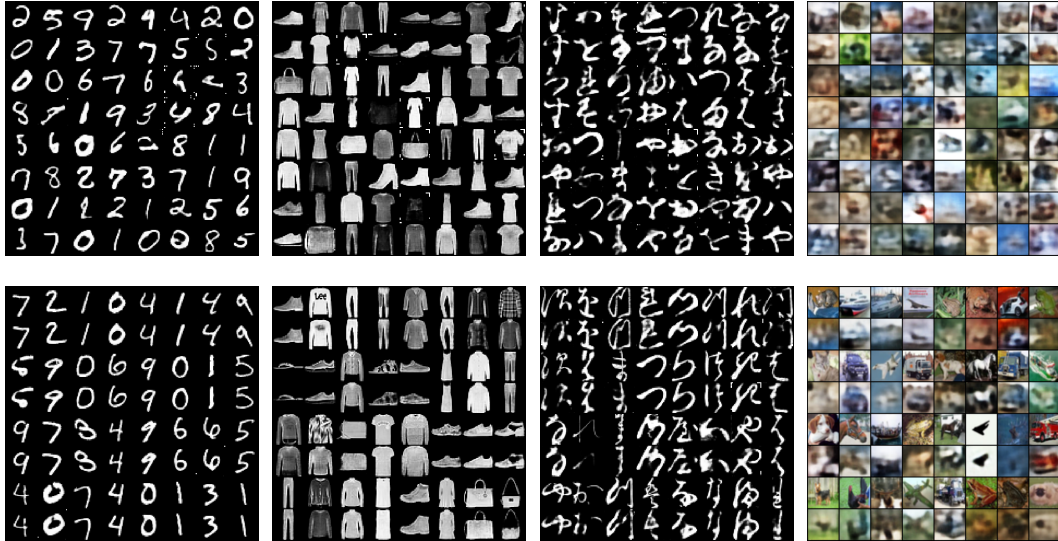


Figure 12: Samples and reconstructions for AEF-corner with a latent dimensionality of 32 for the MNIST datasets, and 64 for CIFAR. One can notice artifacts in the corners of the samples.



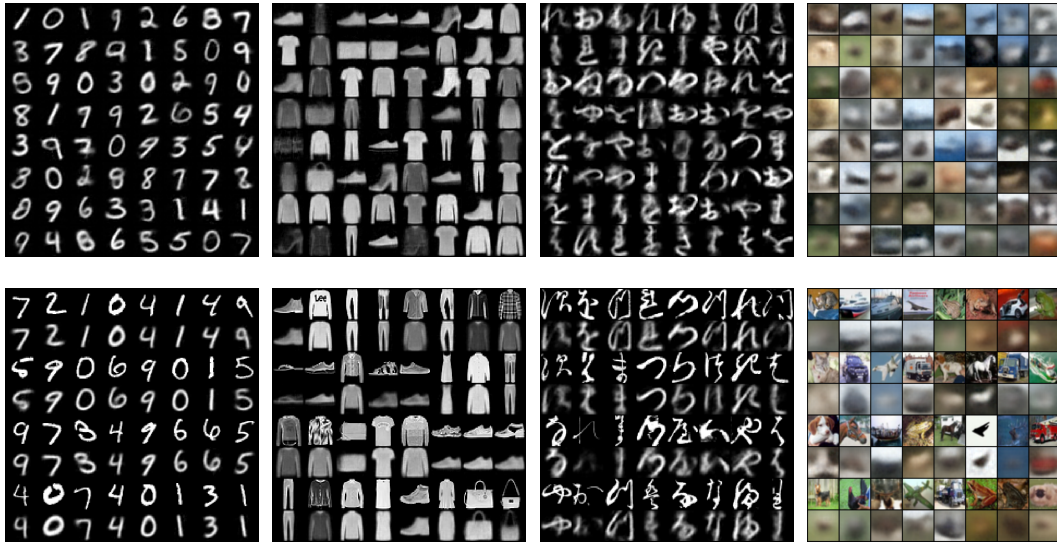


Figure 13: Samples and reconstructions for VAE-IAF-MAF with a latent dimensionality of 32 for the MNIST datasets, and 64 for CIFAR.

## D.2 Denoising

This section presents additional results and figures comparing the denoising performance of AEFs to baseline models, specifically to a VAE with IAF posterior flow and MAF prior flow, and a standard autoencoder trained. Figure 14 presents the mean reconstruction error for increasing levels of noise for the MNIST, FashionMNIST and KMNIST datasets. Figure 15 shows examples of reconstructions by these models for the same noise levels.

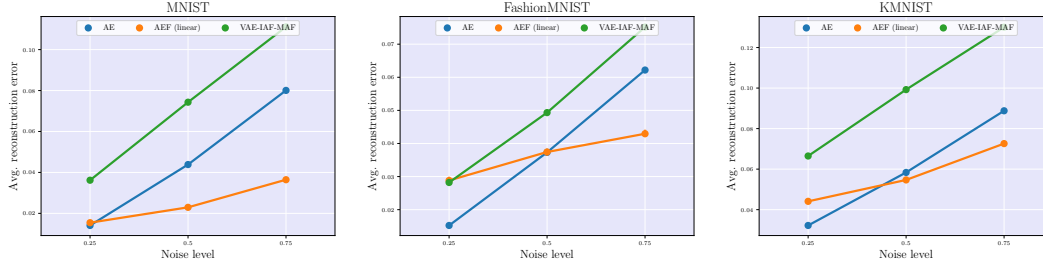


Figure 14: Mean squared error between reconstructions based on a noisy input and the original sample for increasing levels of noise. Averaged over five runs. Confidence intervals are present but too small to see. The number of latent dimensions for all models was set to 32.

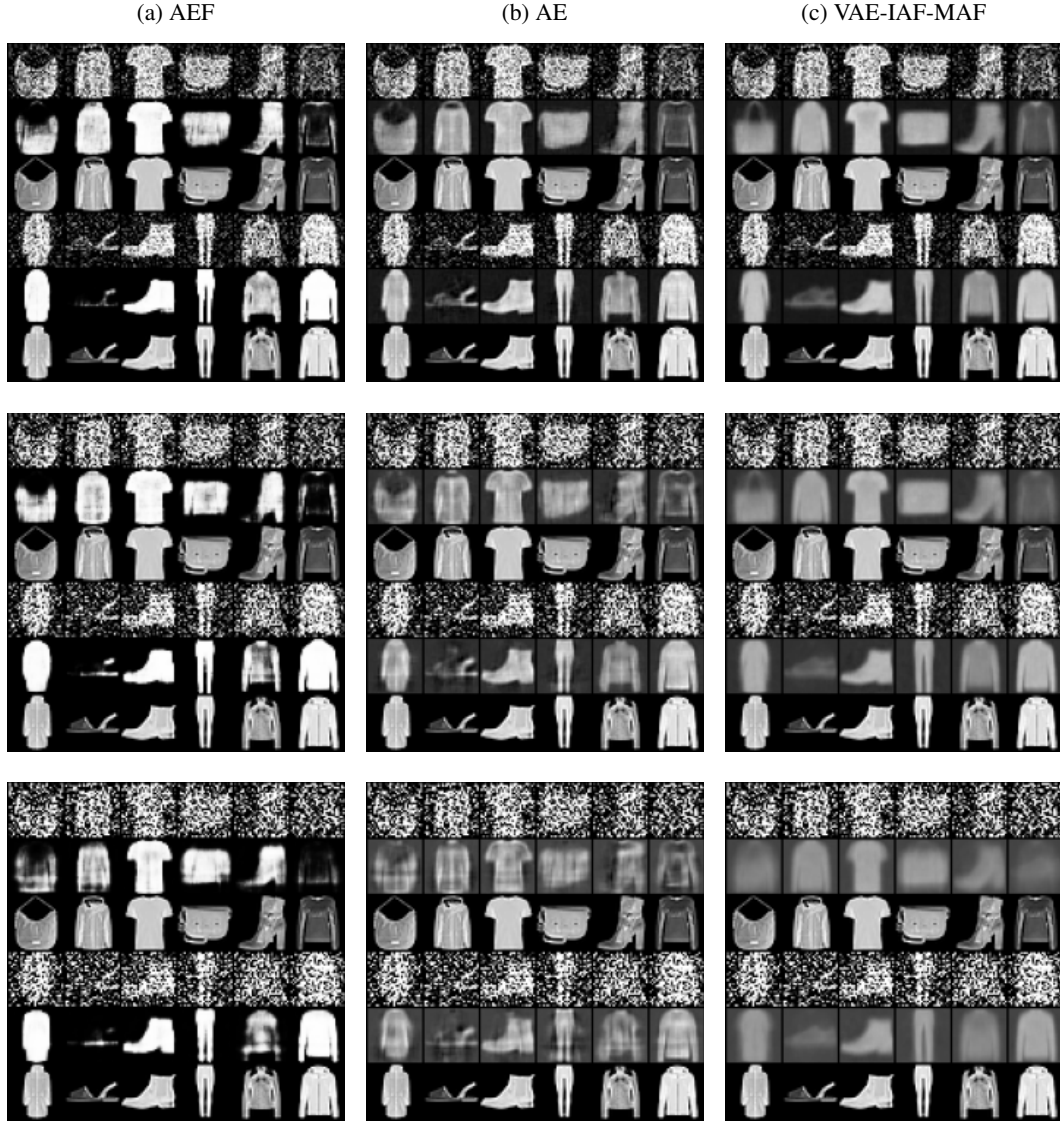


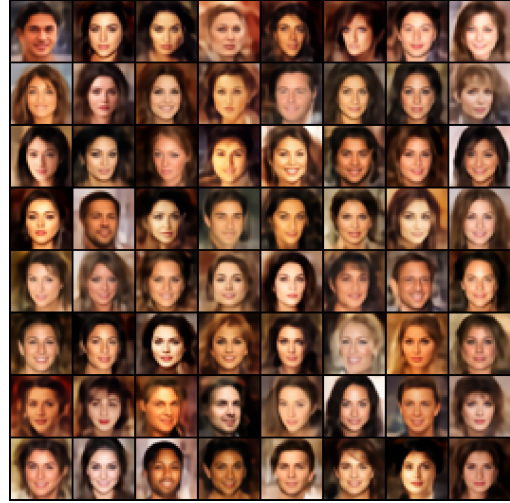
Figure 15: Sample reconstructions by AEF, AE and VAE-MAF-IAF models with a latent dimensionality 32 for increasing levels of noise. For each triplet of samples, the first row gives the noisy input, the second row the reconstruction, and the third row the original sample. The standard deviation of the noise distribution is equal to 0.25, 0.5 and 0.75 for the first, second, and third row of images respectively.

### D.3 Generative modeling

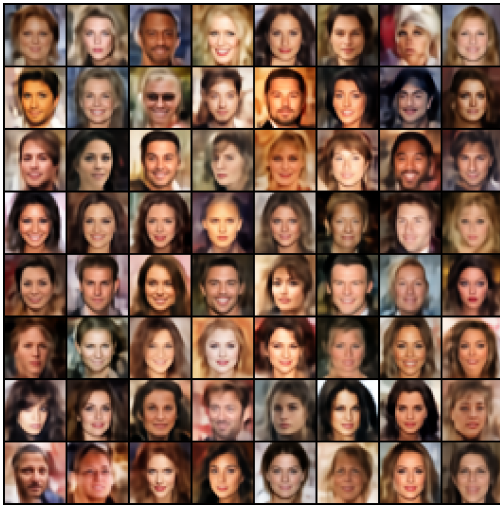
We report samples for AEF-linear with 256 latent dimensions at different temperatures in Figure 16. Figures 17 and 18 show a comparison in terms of reconstruction and sample quality respectively, between AEF-linear and VAE-IAF-MAF for different latent dimensions.



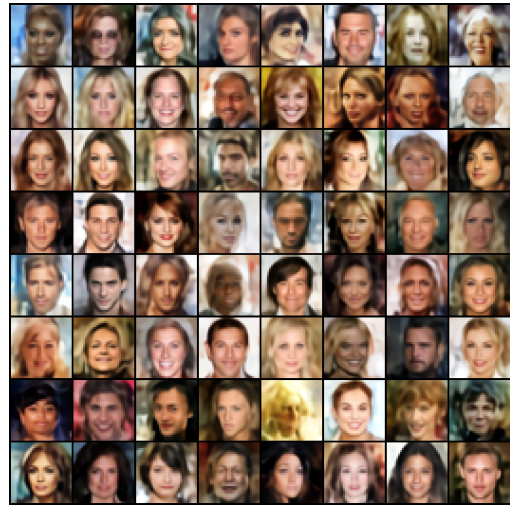
(a) Temperature 0.4



(b) Temperature 0.6



(c) Temperature 0.8



(d) Temperature 1.0

Figure 16: Samples from a linear AEF with a latent dimensionality of 256 trained on  $32 \times 32$  samples from CelebA-HQ. A temperature of 1 was used.





Figure 17: CelebA-HQ reconstructions from a linear AEF (top row) and VAE-IAF-MAF (bottom row) with varying numbers of latent dimensions.



Figure 18: CelebA-HQ samples from a linear AEF (top row) and VAE-IAF-MAF (bottom row) with varying numbers of latent dimensions. A temperature of 1.0 was used.